ESR and optical absorption of bound-small polarons in $YAlO_3$

O. F. Schirmer,* K. W. Blazey, and W. Berlinger
IBM Zurich Research Laboratory, 8803 Rüschlikon, Switzerland

R. Diehl
Institut für Angewandte Festkörperphysik der Fraunhofer Gesellschaft, D-78 Freiburg, Federal Republic of Germany
(Received 18 November 1974)

Nominally undoped $YAlO_3$ shows broad intense absorption bands in the visible after irradiation with visible and near uv light at 77 K; they become especially strong after subsequent irradiation with near ir. The bands could be correlated with an ESR spectrum arising from holes, which are trapped at O^{2-} ions near unidentified defects or are possibly self-trapped. A similar spectrum appeared after heating to 200 K. It was rather weak and a corresponding absorption could not definitely be identified. The optical absorption is explained by treating the holes together with their accompanying lattice distortions as small polarons. A theory based on this model is presented which is a generalization of an earlier treatment of bound-small-polaron absorption. Information on further absorption of the crystals up to 4 eV is given. Most of this absorption is related to the formation or quenching of the polaron bands.

I. INTRODUCTION

After suitable irradiation, many oxide materials show broad absorption bands in the visible. Such phenomena have been investigated especially thoroughly in MgO and other alkaline-earth oxides.[1-6] It was found that in these compounds most of the coloration is due to holes trapped at O^{2-} ions near defects charged negatively with respect to the lattice. Attempts to explain the optical absorption of these trapped hole centers as transitions between the p levels of the O^- ions,[3,5,6] split by the defect electric field, have met with difficulties for two reasons. Firstly, because transitions between the p levels are forbidden they cannot cause the observed high oscillator strengths of the bands, and secondly, because this interpretation could be reconciled with the ESR results on these centers only by invoking unreasonably high O^- spin-orbit splittings.

Another model[4] ascribed the absorption to transitions between molecular-orbital states formed from a linear combination of the orbitals of equivalent O^{2-} ions around the defect. This interpretation, based on an analysis of a magnetic-circular-dichroism (MCD) study, was found to be inconsistent with the model of a localized hole.[7]

Recently, a new approach[8] has been proposed which explains the experimental findings without running into the aforementioned inconsistencies. It is based on the assumption, motivated by experimental observations,[9] that the hole trapping is accompanied by a lattice distortion around the trapping site. The hole together with this lattice relaxation can be understood as a small polaron,[10] bound to the defect. The optical absorption is explained by a light-induced transfer of the hole from one to another equivalent O^{2-} site near the defect. Peak energies and widths of the bands are essentially determined by the lattice distortion.

In the present paper we shall generalize this concept and apply it to the perovskitelike compound $YAlO_3$ where a radiation-induced coloration is correlated with newly found trapped hole centers. Investigation of this system was initiated because laser action of rare-earth ions in $YAlO_3$ (Ref. 11) is hindered by the coloration of the crystals due to the pump light. The origin of this process is not yet understood. We have reason to believe, however, that polaronic absorption not only leads to coloration of nominally undoped $YAlO_3$ as shown here, but most probably also contributes to the similar effects in rare-earth-doped material. uv-induced absorption bands in undoped $YAlO_3$ similar to those analyzed here have recently been published by Bernhardt.[12] However, no explanation of their origin was given.

We shall first report on the crystal structure of $YAlO_3$, then describe the ESR results and from them deduce the structure of the trapped hole centers. Then the optical absorption is shown and discussed on the basis of the model of the hole centers. To this end the essential features of bound-small-polaron absorption are derived in a way which appears to be simpler and more general than the earlier discussion.[8]

II. PROPERTIES OF $YAlO_3$ AND EXPERIMENTAL DETAILS

$YAlO_3$ crystallizes in a slightly distorted perovskite structure.[13] Figure 1 shows the arrangement of the ions in the orthorhombic unit cell orthogonally projected onto the (001) plane. It contains four perovskitelike pseudocells. The cell dimen-

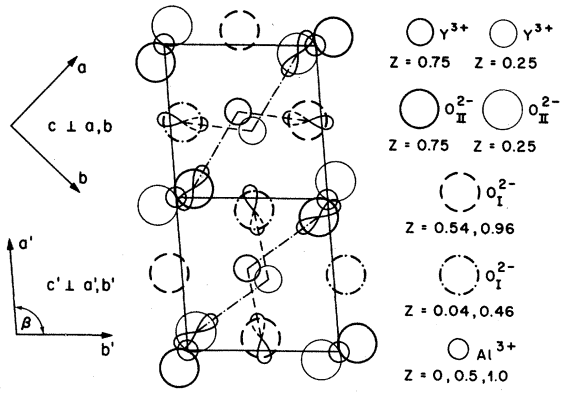

FIG. 1. Arrangement of ions in the unit cell of $YAlO_3$. In order to show the distortion clearly, the b/a ratio has been exaggerated. Therefore the bond angles are not necessarily equal to the real ones. This unit cell comprises four perovskitelike pseudocells, the axes of which are indicated by a' and b'. The dashed lines mark the shortest Y^{3+}-O_I^{2-} distances; the dash-dotted lines, the corresponding distances to O_{II}^{2-}. The p_z orbitals capable of trapping the holes are indicated.

sions as well as the coordinates of the ions, as determined by Brandt and Diehl,[14] are shown in Table I. The symbols used are defined in Fig. 1.

The crystals investigated in the present study were obtained from Kristalloptik GmbH, Munich. Some of the specimens were growth twins, the twin plane being the plane containing b' and c' in Fig. 1. Only untwinned parts of the crystals were used for the ESR experiments. As obtained, the crystals were clear, but after irradiation at 77 K and subsequent heating to ambient temperature they showed a yellowish tint due to an absorption in the blue. Upon irradiating the crystal at 77 K with blue light this absorption band is quenched and the crystal turns grey. The yellow color returns on warming to room temperature again. This color cycle was investigated by ESR at K band at various temperatures using filtered light of a 200-W mercury arc or a 450-W xenon arc.

The optical absorption spectra of the crystal in its various colored states were taken with a 0.5-m Ebert spectrometer and a PbS cell with the crystal mounted in a cold-finger cryostat. The wavelength-modulated absorption spectra were obtained with a double-beam arrangement similar to that described by Shaklee and Rowe.[15] A Spex 1402 spectrometer was used with a 4-Å passband and a 4-Å modulation depth.

III. ESR STUDY OF IRRADIATED UNDOPED $YAlO_3$

A. Results

Depending on the temperature and the irradiation history of the crystal, two different centers with g values near two are observed in ESR. Figure 2 shows representative spectra of these centers after irradiation at 77 K with near uv or visible light. Both resonances are characterized by pronounced hyperfine (hf) interaction. The observed splitting into 11 equidistant lines is clearly due to interaction with two ^{27}Al ($I = \frac{5}{2}$; 100% abundant) nuclei. In $YAlO_3$, only spins at O^{2-} sites see two Al nuclei nearly equivalently, the Al^{3+}-O^{2-} distances differing by less than 1% from the average value 1.91 Å. As will be shown below, the observed g shifts indicate that the paramagnetic entity is a hole trapped at such oxygen sites. The angular dependence of the centroids of the hf packets is shown

TABLE I. Crystallographic data of $YAlO_3$.

Space group		D_{2h}^{16} – Pbnm		
Unit-cell dimensions				
$a = 5.180 \pm 0.002$ Å $b = 5.330 \pm 0.002$ Å $c = 7.375 \pm 0.002$ Å				
Pseudocell dimensions				
$a' = b' = 3.716 \pm 0.002$ Å $c' = 3.688 \pm 0.002$ Å $\beta = 91.62°$				
Coordinates of ions				
Ion	Position	x	y	z
Y^{3+}	4(c)	-0.0104 ± 0.0002	0.0526 ± 0.002	0.25
Al^{3+}	4(b)	0.5	0	0
O_I^{2-}	8(d)	-0.297 ± 0.002	0.293 ± 0.002	0.044 ± 0.002
O_{II}^{2-}	4(c)	0.086 ± 0.002	0.475 ± 0.002	0.25

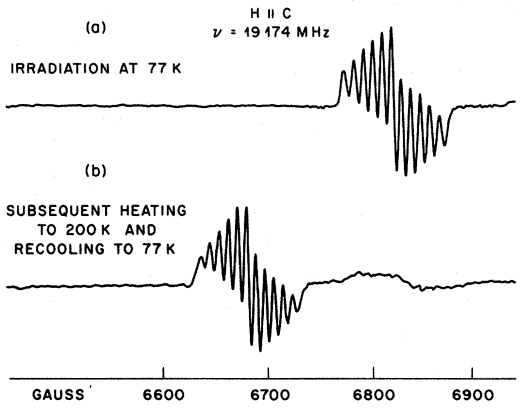

FIG. 2. ESR spectra of $YAlO_3$, uv irradiated as well as measured at 77 K for $H||c$: (a) center I; (b) centers II and I; gain increased 10×.

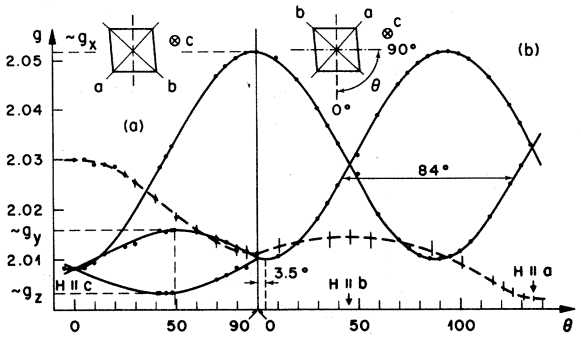

FIG. 3. Angular dependences of the ESR spectra of centers I (full lines) and II (dashed lines) for a rotation of $\vec{H}$: (a) in the plane indicated by dashes in the inset, and (b) in a plane perpendicular to c.

in Fig. 3 for the rotations of $\vec{H}$ indicated in the insets. The lowest extremum is found at $g_1 = 2.0049$ for $\vec{H}$ $41 \pm 0.5°$ away from the c axis in the plane indicated by a dashed line in Fig. 3(a). The value of g_1 is close to the smallest g value measured for O^- centers in many other hosts, e.g., 2.0032 for V^- in MgO.[16] This small deviation is certainly due to the fact that the plane of rotation [dashed in Fig. 3(a)], which had to be chosen for experimental reasons, does not contain the corresponding principal axis of the g tensor. This is consistent with the extrema for a rotation of $\vec{H}$ in a plane perpendicular to c [Fig. 3(b)] being displaced by $3.5° \pm 0.5°$ from the "dashed" plane.

The other extrema in the angular rotation plot in Fig. 3(a), at 2.0163 and 2.0511, are also close to principal values of the g tensor, since only very slight changes of line positions were observed upon varying the direction of $\vec{H}$ near these extrema in a plane perpendicular to the "dashed" one. The principal values of the g tensor are therefore approximately

$$g_z = 2.0049 \pm 0.0020,$$

$$g_y = 2.0163 \pm 0.0020,$$

$$g_x = 2.0511 \pm 0.0005.$$

The directions at which these values are measured are indicated in Fig. 3(a). The hf splittings are also somewhat angular dependent. Analogous approximations to the principal values are

$$A_z = 4.4 \pm 0.1 \text{ G},$$

$$A_y = 4.5 \pm 0.1 \text{ G},$$

$$A_x = 3.6 \pm 0.2 \text{ G}.$$

It should be noted that for a rotation around c the entire spectrum just described consists of two equivalent branches rotated with respect to each other by $84 \pm 1°$ [Fig. 3(b)].

Upon heating the crystal to near 200 K, after irradiation at 77 K, the previously described spectrum I vanishes and a new spectrum II appears having features similar to spectrum I. Spectrum II persists on recooling down to 77 K and I returns to only a small fraction of its initial strength. Further irradiation at 77 K destroys II, however, and I is restored to its full strength again. If the crystal is irradiated during the heating cycle, I is formed in preference to II, and decays into II after turning off the irradiation.

Not all the holes freed from I during heating end up in II because the total intensity of I and II after cooling down to 77 K is less than the original intensity of I. This is partly due to migration of the holes to another site, leading to ESR signals, which have not yet been analyzed. Another portion of the holes seems to vanish by recombination with electrons as evidenced by yellowish thermoluminescence. Above about 200 K both centers decay rapidly.

The superposition of spectra I and II for $H||c$ after the described heating to 200 K and cooling to 77 K is shown in Fig. 2(b). Again there is hf interaction with two equivalent ^{27}Al nuclei, identifying O^{2-} as the site of the unpaired electron in center II also.

The angular dependence of the hf-packet centroids of center II (dashed lines in Fig. 3) could be determined with less accuracy than that of center I, firstly because of interference of the packets with those of I, and secondly because the branches near low g values [Fig. 3(b)] seemed to consist of two packets which could not be disentangled. The principal g values here are

$$g_\zeta = 2.0030 \pm 0.0010,$$

$$g_\eta = 2.0140 \pm 0.0020,$$

$g_\xi = 2.0345 \pm 0.0005$.

ζ lies along a; ξ along c, and η along b. The corresponding A tensor for center II is given by

$A_\zeta = 5.3 \pm 0.1$ G,

$A_\eta = 5.4 \pm 0.2$ G,

$A_\xi = 4.2 \pm 0.1$ G.

B. Interpretation of the spectra

1. Model of centers

In these centers we are clearly dealing with paramagnetic entities centered at single O^{2-} ions of the $YAlO_3$ lattice. The positive g shifts (see Sec. III B 2) point to the capture of a hole at such sites during irradiation, converting O^{2-} to O^- (p^5). From the different angular dependences of centers I and II, Fig. 3, it follows that the hole is captured at different O^{2-} sites in each case. The spectra are consistent with the hole of center I being trapped at O^{2-} ions in Al^{3+}-O^{2-}-Al^{3+} chains perpendicular to c, whereas for center II the chain is parallel to c. This is shown in Fig. 1, where it is also indicated that not all O^{2-} ions in "perpendicular" and "parallel" chains, respectively, are energetically equivalent, as will be discussed below. It is observed that the z and ζ axes of centers I and II, respectively, roughly point from the corresponding O^{2-} sites towards the Y^{3+} sites of the crystal. Since in such situations the smallest g values are measured along the axes of the p_z orbitals in which the hole is accommodated, these are oriented as sketched in Fig. 1. The p_z orbitals are apparently stabilized in this configuration by defects at Y^{3+} sites, different for centers I and II, charged negatively with respect to the lattice. It could, however, also be possible that the hole is self-trapped or rather stabilized by the inequivalence of the O^{2-} ions without the presence of a defect. Since this could not be established definitely, for simplicity we shall assume in the following that the hole is trapped by a defect.

The angle between the two branches in Fig. 3(b), $84° \pm 1°$, is different from 90° expected for an ideal perovskite lattice. This difference, $6° \pm 1°$, cannot be attributed alone to the axes a' and b' being inclined with respect to each other by 91.6° (shown exaggerated in Fig. 1). Further displacement of the ions, as given by the free parameters in Table I and distortions away from the crystallographic positions, caused by the hole capture, can serve to explain the remaining discrepancy.

If all O_I^{2-} ions were energetically equivalent, one should observe four branches in Fig. 3(b), corresponding to the four magnetically inequivalent O_I^{2-} sites in Fig. 1, two of them belonging to the upper and two to the lower pseudocells shown. The experimentally determined orientations of the g_z axes with respect to the crystal a and b axes, known from an x-ray analysis of the investigated specimens, leads to the conclusion that the O^{2-} ions connected by dashes to the Y^{3+} sites are energetically most favorable. From the determined ion positions (Table I) it was calculated that these O^{2-} ions are closer to the defects, supposed to be at Y^{3+} sites, than the alternative O_I^{2-} ions. This site preference could be due to the Coulomb attraction between hole and defect.

Similar arguments hold for the type-II centers. Here only the O^{2-} ions at which the dash-dotted lines originate have been found to trap holes. Again these O^{2-} ions have shorter distances to the (Y^{3+}) defect sites than the other O_{II}^{2-} ions. The angle between the dash-dotted lines in the upper and lower pseudocells in Fig. 1 is smaller than the corresponding angle between the dashed lines. This can explain why the two expected branches were not resolved for type-II centers in Fig. 3(b).

2. Interpretation of the g and A tensors

The local environment of an O^- ion of center I is shown in Fig. 4. The given bond lengths correspond to the crystallographic values of center I, whereas the bond angles have been approximated by 90°. The crystal field splits the p states such that the p_z orbital lies lowest.

Angular momentum is quenched in this state and the deviations of the g values g_x, g_y and g_ξ, g_η from the free spin values are due to the admixture of p_x and p_y into the ground state by spin-orbit coupling[17]:

$$\Delta g_i = -2\lambda_O - /E_i, \quad i = x, y, \xi, \eta, \tag{1}$$

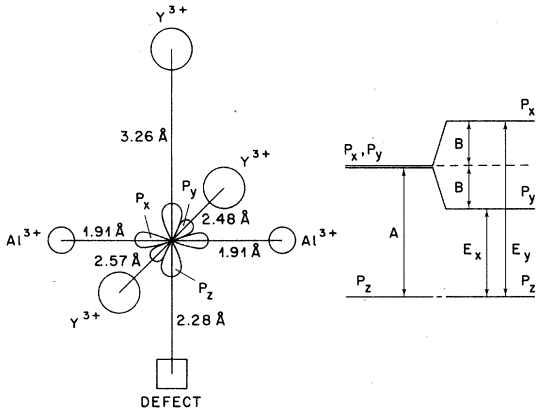

FIG. 4. Environment of an O^- ion (center I) in $YAlO_3$. All bond angles have been taken to be 90°. At the right-hand side the level scheme of $O^- p_z$ orbitals originating from this crystal field is indicated.

where λ_{O^-} is the spin-orbit coupling constant of O^-, and E_i are the energy separations of the higher p states from p_z. Since $\lambda_{O^-}<0$, $\Delta g_i>0$ as observed. Using $\lambda_{O^-}=-0.016$ eV,[18] one derives, with the observed Δg_x and Δg_y,

$$E_x \approx 0.7 \text{ eV}, \quad E_y \approx 2.3 \text{ eV}.$$

We shall now show that the large difference between g_x and g_y and between g_ζ and g_η is consistent with the structure of the centers derived in Sec. IIIB1. From the model given in Fig. 4, the axial crystal-field parameter A and the orthorhombic one B, have been calculated assuming that the Al^{3+} and Y^{3+} neighbors of O^- are purely ionic:

$$A = (0.211 - Z\times 0.015)e\langle\rho^2\rangle,$$

$$B = 0.098e\langle\rho^2\rangle.$$

The numbers in these expressions are given in $Å^{-3}$. $\langle\rho^2\rangle$ is the expectation value of the square of the hole-nucleus distance in the O^- ion and $Z\times e$ is the real charge of the defect. $Z=0$ corresponds to the Y^{3+} vacancy and $Z=3$ would formally mean the self-trapped hole.

From $E_y/E_x=(A+B)/(A-B)$ (see Fig. 4), one finds with Eq. (1),

$$2.71<\Delta g_x/\Delta g_y<3.88.$$

The lower bound applies for $Z=0$, the upper one for $Z=3$. The experimental ratio is ~3.5, which falls into the range of the calculated values. The model, however, neglects any distortion of the crystallographic bond lengths. It has been shown[9] that for such centers a lattice relaxation caused by hole trapping will increase the axial crystal-field parameter A, whereas the orthorhombic part B tends to be less affected. The orthorhombicity therefore will be relatively less important and the predicted ratio $\Delta g_x/\Delta g_y$ will thus tend to be too high.

In the analogous crystal-field model for center II, $\Delta g_\xi/\Delta g_\eta$ is predicted to be 3.20 for $Z=0$ and 6.35 for $Z=1$, if again distortion is not considered. The experimental ratio, ~2.8, agrees well with the result for $Z=0$. So one might infer that the defect here is an Y^{3+} vacancy. Since the g shifts are larger for center I, it appears that Z is higher there.

As will now be demonstrated the hf interactions are also in accord with the described models of centers I and II. Taking the average of the principal A_i values of center I, one obtains a, the Fermi contact interaction to be

$$|a| = \tfrac{8}{3}\pi\gamma_e\gamma_n\hbar^2|\Psi(0)|^2 = 4.2\pm 0.1 \text{ G}$$

(γ_e, γ_n magnetogyric ratio of electron and nucleus, respectively). So there is a finite isotropic hf interaction, proportional to $|\Psi(0)|^2$ of unpaired spins at the ^{27}Al nuclei, although they are lying on or near a nodal plane of the O^-2p_z function.

From similar situations[19] one infers that this is caused by exchange polarization of the Al^{3+} closed s shells by the O^- unpaired electron. In such cases a is expected to be negative, taking the signs of nuclear and electronic magnetic moments as positive. As will be shown shortly, this is borne out by the experiment. The anisotropy is caused by the dipolar interactions b and e which are always positive. From[18]

$$A_x = a + 2b,$$

$$A_y = a - b + e,$$

$$A_z = a - b - e,$$

one finds that $a<0$, since $|A_x|<|A_y|, |A_z|$. This is consistent with the Al nuclei lying near nodal planes of the p_z orbitals, as shown in Fig. 1. Since the hf interaction has not been observed to vanish for any angle, all A_i have the same sign. This leads to

$$a = -4.2\pm 0.1 \text{ G},$$

$$b = 0.3\pm 0.2 \text{ G},$$

$$e = 0.05\pm 0.2 \text{ G}.$$

In an earlier study of hole centers in ZnO it has been shown[18] that b and e are given by

$$b = \gamma_e\gamma_n\hbar^2(1/l_1^3 - \tfrac{6}{5}\langle\rho^2\rangle/l_1^5),$$

$$e = \gamma_e\gamma_n\hbar^2(\tfrac{3}{5}\langle\rho^2\rangle/l_1^5),$$

where l_1 is the distance between O^- and Al nuclei. From the experimental value of b one finds from these expressions 2.40 Å as a lower limit for l_1, if $\langle\rho^2\rangle = 0.85$ $Å^2$ (Ref. 18) is used. This points to a sizable distortion of the Al^{3+}-O^{2-} bond lengths from the crystallographic distance 1.91 Å. The ratio e/b is then found to be 1/10, which is not inconsistent with the experimental results.

An analogous analysis of the hf interaction in center II leads to the following values:

$$a = -5.0\pm 0.1 \text{ G},$$

$$b = 0.4\pm 0.1 \text{ G},$$

$$e = 0.05\pm 0.2 \text{ G}.$$

$|a|$ is somewhat larger than in the previous case. A possible explanation is that an Al^{3+}-O^{2-}-Al^{3+} chain is somewhat shorter along c (center II) than perpendicular to it (center I).[13] A smaller distortion of center II, compared to I, is an alternative explanation.

3. *On the relation between centers I and II*

In center II the hole certainly has a lower energy than in I, because I vanishes in favor of II upon heating and subsequent cooling. This is in accordance with the determination of the higher charge deficiency of defect II, $Z = 0$, inferred from its g shifts in the previous section. Since I, however, is created preferentially during irradiation at any temperature below 200 K, holes apparently have a higher capture cross section at defects corresponding to I, or such defects are more numerous. This conversion from I to II is quite analogous to that observed for the transformation of V_k centers into V_F centers in alkali halides.[20] The V_k centers, preferentially created at low temperature by x irradiation, vanish with rising temperature in favor of the more stable V_F, where the hole is not self-trapped but bound to an alkali vacancy.

It is interesting to observe that the transformation from I to II has a lower threshold than thermal excitation of the hole from that O^{2-} ion where it is trapped to neighboring O^{2-} ions. The fact that no such thermally excited hole states are observed up to 200 K, above which the centers decay, puts a lower limit to the energy difference between lowest and next most favorable O^{2-} ions near a type-I defect to be about 0.1 eV.

A remark is appropriate concerning the fact that different types of O^{2-} ions trap the holes near defects producing either center I or II. This apparently shows that there is a reaction of the lattice to the kind of defect brought into the crystal. If the two defect species react in a different way with O^{2-} ions I or II, respectively, the relative trapping energies of ions I and II can be different.

IV. OPTICAL ABSORPTION OF IRRADIATED UNDOPED $YAlO_3$

A. Results

The optical absorption spectrum of $YAlO_3$ between 1 and 3 eV at 80 K is shown in Fig. 5 after various stages of irradiation. Bands P_1 and P_2 are formed with irradiation from a Hg arc filtered through a 3-cm $CuSO_4$ aqueous solution followed by a series of glass filters with increasing energy cutoffs. Each curve is indicated by the high-energy cutoff wavelengths of the glass filters used. By far the largest increase occurs, however, after subsequent removal of all the filters and allowing irradiation with complete Hg arc light including the infrared (ir). The growth of this absorption was found to be directly related to the formation of center I in the ESR. In fact a linear relation was found to exist between them as shown in Fig. 6 and all further discussion will assume that these bands are due to optical transitions within center I.

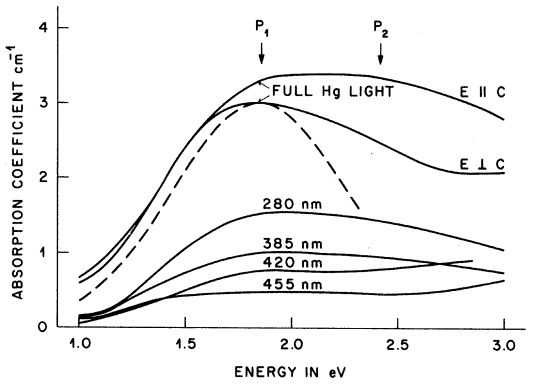

FIG. 5. Lower curves: unpolarized optical absorption of undoped $YAlO_3$ in the range 1–3 eV after several irradiation steps with filters having the indicated high-energy cutoffs. The two uppermost curves, taken after irradiation with the full Hg light including the ir, show the polarization of the absorption. The dashed band shows one representative theoretical bound-small-polaron absorption band.

The optical absorption at higher energies is shown in Fig. 7 where the wavelength-modulated spectra of the crystal for both polarizations with respect to the crystal c axis are given as a function of irradiation. It is seen that band A which gives the crystal a yellow tint at room temperature is quickly quenched and presumably releases the holes which afterwards can be trapped to form center I. Simultaneously several other bands change in intensity as the summary in Table II indicates, but none of them changes in the same way

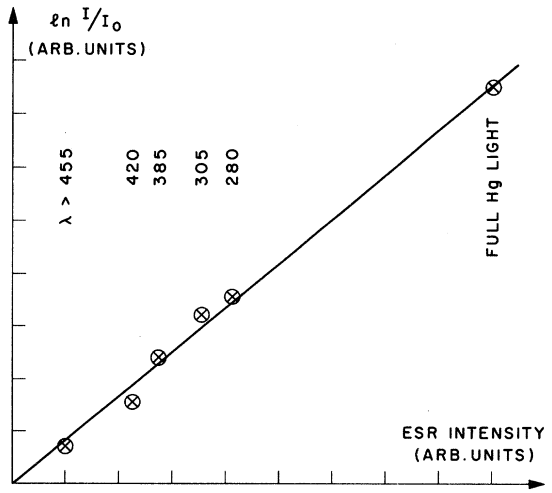

FIG. 6. Linear relationship between the optical extinction at 1.85 eV and the intensity of the ESR of center I. The designation of the points is analogous to that given in Fig. 5.

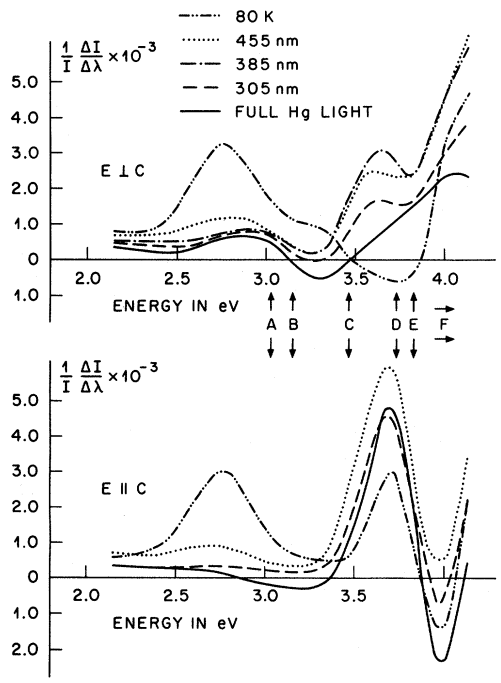

FIG. 7. Polarized modulated absorption of undoped $YAlO_3$ after the indicated irradiation steps. 80 K: cooled to 80 K in the dark; 455 nm: irradiated with Hg arc light filtered with $CuSO_4$ solution and 455 nm cutoff filter; 385 nm: same, with 385-nm cutoff; 305 nm: same, with 305-nm cutoff; full Hg arc light.

as bands P_1 and P_2. Therefore these bands are the only ones directly correlated with center I up to 4 eV.

B. Interpretation of the optical absorption in the visible

1. General remarks on bound-small-polaron absorption

It has just been shown that bands P_1 and P_2 are correlated to trapped hole centers of type I. The rather high intensity of P_1 and P_2 can only be explained by electric-dipole active processes. We therefore discard transitions between the O^-p levels at a single site as an explanation for the bands, although at least one of them is expected in the required energy range (see Sec. III B 2), since such transitions are not electric dipole active. These bands P_1 and P_2, will therefore be discussed here as bound-small-polaron optical absorption. This approach successfully explained the absorption of holes trapped in $MgO:V^-$-type centers.[8] The present discussion must be less detailed, however, because $YAlO_3$ has lower microscopic symmetry than MgO.

If a hole is captured at an O^{2-} ion near a defect, binding energy can be gained by distortion of the lattice, and the vibrations of the hole-lattice system will now be excursions from the new equilibrium positions of the nuclei. This distortion can lead to trapping at one of several equivalent sites

TABLE II. Optical absorption bands of nominally undoped $YAlO_3$ at 80 K.

Designation of band	Energy (eV)	Polarization with respect to c axis	Formation	Quenching
P_1	1.85	∥ > ⊥	Pump into bands A, C, D, F	Warming
P_2	2.35	∥	Pump into bands A, C, D, F	Warming
A	3.03	• • •	Present before irrad.; warming	Pump into A
B	3.15	⊥	Pump into A	Warming
C	3.47	⊥	Present before irrad.; warming	Pump into A
D	3.73	⊥	Max. intensity at 385-nm irrad.	(1) irrad. into D (2) $\lambda > 700$ nm
E	3.83[a]	∥	Partly present before irrad., pump into A, D, F subsequent $\lambda > 700$ nm	Part. quenched by warming
F	> 4.00	• • •	Pump into A	Pump into F

[a] There is additional fine structure to this band at 3.39, 3.51, and 3.53 eV.

if the stabilizing energy is large compared to energies corresponding to symmetry-restoring processes, e.g., tunneling. In the case studied here, there are twelve O^{2-} ions around a defect on a Y^{3+} site which, in principle, can trap holes. In each case the hole will be accommodated in a p_z-type orbital pointing towards the defect, the remaining p orbitals, p_x and p_y, lying higher in energy because of the defect electric field. Since the perovskite structure is distorted in $YAlO_3$, the energy of the hole in a p_z orbital at site i, ϵ_i, can be different from ϵ_j, the corresponding energy at site j, and phonon-induced relaxation can quickly transfer the hole after trapping to the site of lowest energy.

The vibrational potential energies of the hole-lattice system are best described by employing a configuration coordinate scheme. We make the simplification[21] generally used, that the force $-VQ$ driving the system from the undistorted to one of the distorted configurations, can be described by one configuration coordinate Q only. V is a measure of the strength of hole-phonon coupling. The coordinate Q, in general, can be one, two, or three dimensional. We need not specify this since the problem can be reduced in any case to a one-dimensional one, as will be shown shortly. After application of the hole-phonon interaction the system will exhibit a minimum in configuration space for each trapping site in the crystal.[8] If the system was harmonic before the hole-phonon interaction, i.e., if its vibrational potential energy was given by $(\frac{1}{2}\mu\omega_0^2)Q^2$, it will remain so around the new minima, as long as the coupling is linear and strong. Moreover the vibrational potential energies around the new minima will again have the same curvatures as $(\frac{1}{2}\mu\omega_0^2)Q^2$, all minima being equivalent in their vibrational properties. Cuts through such potential energy surfaces, along the direction connecting two neighboring minima, will always appear as in Fig. 8. This means that if the hole is trapped at site α in the crystal, the vibrational potential energy of the entire system is given by parabola α. Curve β_i shows the corresponding energy for the case where the hole is transferred to and trapped at site β_i. The distance between the minima of both curves is related to the hole-phonon coupling strength.

For the case of such harmonic potential, the state of the hole-phonon system can be described by the product $|\alpha\rangle|\mu\rangle$, where $|\alpha\rangle$ is the wave function of the hole at site α, and $|\mu\rangle$ one possible vibrational state of the system if the hole is trapped at site α. μ is assumed to be an appropriate collection of vibrational quantum numbers classifying that state. The generalization to the cases when the hole is trapped at sites β_i is given by $|\beta_i\rangle|\nu_i\rangle$,

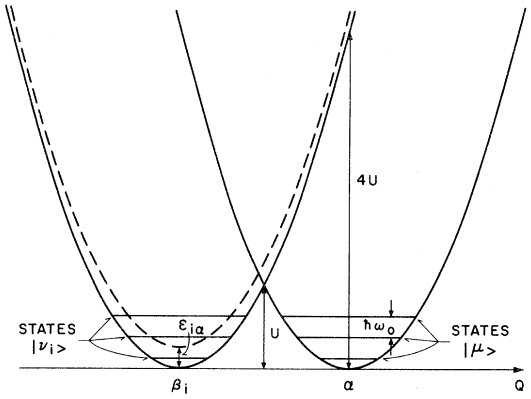

FIG. 8. Linear configuration coordinate diagram with energy surfaces centered around sites α and β_i. If the sites are inequivalent the hole energy at β_i can be higher by $\epsilon_{i\alpha}$.

$|\beta_i\rangle$ designating the hole state at β_i and $|\nu_i\rangle$ the corresponding vibrational state of the system.

The transfer of a hole from α to any of the sites β_i can be induced by light. In the frequency range we are studying, only electronic transitions are caused by the interaction with light. So the final state in a transition from $|\alpha\rangle|\mu\rangle$ will be $|\beta_i\rangle|\mu\rangle$, where the vibrational state is unchanged. For the calculation of the energy of the final state it is more convenient, however, to express $|\mu\rangle$ by an expansion into eigenstates of the system if the hole is at β_i:

$$|\mu\rangle = \sum_{\nu_i} |\nu_i\rangle\langle\nu_i|\mu\rangle \ .$$

The system has thus been excited to a nonstationary phonon state, in which the energies $\epsilon_{i\alpha} + E_{\nu_i}$ occur with the weight $|\langle\nu_i|\mu\rangle|^2$. Here $\epsilon_{i\alpha}$ is the difference of hole energies ϵ_i and ϵ_α (see Fig. 8); E_{ν_i} is the energy of the vibrational system in state $|\nu_i\rangle$.

A discussion of the overlap integrals $\langle\nu_i|\mu\rangle$ will bring the simplification of the problem to one dimensionality. For the case where Q is two or three dimensional the oscillator eigenfunctions $|\mu\rangle$ and $|\nu_i\rangle$ can be written as double or triple products of linear harmonic oscillator functions, for example, in the three-dimensional case:

$$|\mu\rangle = |\mu_x\rangle|\mu_y\rangle|\mu_z\rangle ,$$

where μ_i denote the appropriate quantum numbers for the component wave functions. Analogous products can be written for the $|\nu_i\rangle$. The directions x, y, and z can now be chosen without loss of generality in such a way that z extends along the direction connecting both wells, and x and y perpendicular to it. The overlap integrals $\langle\nu_i|\mu\rangle$ thus become

$$\langle\nu_{iz}|\mu_z\rangle\langle\nu_{ix}|\mu_x\rangle\langle\nu_{iy}|\mu_y\rangle .$$

Since the wells are equivalent in their vibrational properties, $\langle \nu_{ix} | \mu_x \rangle$ and $\langle \nu_{iy} | \mu_y \rangle$ are unity, if $|\nu_{ix}\rangle$ and $|\mu_x\rangle$ as well as $|\nu_{iy}\rangle$ and $|\mu_y\rangle$ have the same quantum numbers; otherwise these integrals are zero. This means that transitions to final states with changed x- and y-oscillator states are not allowed. The transition probabilities and transition energies thus, in any case, correspond to those expected from the one-dimensional model shown in Fig. 8.

For this case the probability that photons of energy $\hbar\omega = E_{\nu_i} + \epsilon_{i\alpha} - E_\mu$ are absorbed, if the initial state is $|\alpha\rangle|\mu\rangle$, is given by $f(\hbar\omega) = |\langle \mu_z | \nu_{iz} \rangle|^2 \delta(E_{\nu_i} + \epsilon_{i\alpha} - E_\mu - \hbar\omega)$. If $|\mu_z\rangle$ is the ground state of the corresponding oscillator, $|\langle \mu_z | \nu_{iz} \rangle|^2$ is a Poisson distribution[22] which can be approximated by a Gaussian distribution for large hole-phonon coupling, e.g., for high $U/\hbar\omega_0$ in Fig. 8. The envelope of this distribution of discrete frequencies is proportional to[8]

$$I(\hbar\omega) \propto w^{1/2} e^{-w(\hbar\omega - \epsilon_{i\alpha} - 4U)^2} , \tag{2}$$

with $w^{-1} = 8U\hbar\omega_0$. If it is considered that not only the lowest of the possible states $|\mu\rangle$ is occupied initially but that also higher ones are thermally populated, w^{-1} becomes to a good approximation[23]

$$w^{-1}(T) = w^{-1}(0) \coth \hbar\omega_0 / 2kT .$$

In order to describe the experimentally measured energy absorption line shape, $I(\hbar\omega)$ has to be multiplied by $\hbar\omega$.

So far, we have not considered that the hole, after having been transferred to a neighboring O^{2-} ion, has a finite probability amplitude for tunneling to an equivalent O^{2-} neighbor. This tunneling will lead to a chemical splitting of the excited states. The matrix elements describing the exchange interaction between these excited hole-phonon states, $|\beta_i\rangle|\mu\rangle$ and $|\beta_j\rangle|\mu\rangle$, respectively, are given by

$$J_{ij} = \langle \beta_i | \mathcal{H}_J | \beta_j \rangle \langle \mu | \mu \rangle = \langle \beta_i | \mathcal{H}_J | \beta_j \rangle ,$$

since $\langle \mu | \mu \rangle = 1$. The hole and vibrational parts could be separated because the exchange operator $\mathcal{H}_J$ acts only on the hole functions. *The exchange splittings of the excited states can thus be treated without consideration of the vibrational system.*

The polaronic absorption will thus appear as a superposition of Gaussian bands separated by the exchange splittings between the molecular-orbital states formed from the final-hole states at the O^{2-} ions involved. The symmetry of these states will also determine the polarization behavior of the bands. If the ϵ_i differ from site to site, the excited states and their energies are given by the eigenvectors and eigenvalues of a Hamiltonian containing ϵ_i, $\epsilon_j \ldots$ in diagonal positions and J_{ij} in off-diagonal ones.

This part of the discussion is a simplification of the former treatment of the problem,[8] where the moments of the line shapes have been calculated. The physical basis of the derivation is that the system stays in its original vibrational state while the hole is transferred.

The total intensity of the transitions, proportional to

$$\sum_i |\langle \alpha | \langle \mu | - e\vec{x} | \beta_i \rangle | \mu \rangle|^2 ,$$

does not depend on the vibrational properties either, since the dipole operator, $-e\vec{x}$, operates only on the hole functions, and because $\langle \mu | \mu \rangle = 1$. Neither does this intensity depend on the chemical splitting. This is an example of spectroscopic stability.[24] The relevant matrix elements are thus $\langle \alpha | - e\vec{x} | \beta_i \rangle$. They are nonzero because there is a certain admixture of $|\beta_i\rangle$ to $|\alpha\rangle$ and vice versa via the exchange interaction:

$$|\alpha'\rangle = |\alpha\rangle - (J_{\alpha\beta_i}/\Delta E)|\beta_i\rangle ,$$

$$|\beta_i'\rangle = |\beta_i\rangle + (J_{\alpha\beta_i}/\Delta E)|\alpha\rangle .$$

Here the exchange integral $J_{\alpha\beta_i}$ between sites α and β_i in the undistorted configuration enters. By lattice relaxation the exchange contribution is reduced to $(J_{\alpha\beta_i})/\Delta E$, where ΔE is the mean hole excitation energy, $4U + \epsilon_{i\alpha}$, since the exchange operator does not operate on the vibrational states of the lattice. It has been found for MgO:V^- (Ref. 8) that $4U$ is large compared to typical O^{2-}-O^- exchange splittings. Since in $YAlO_3$ the peak positions of P_1 and P_2 lie in the same energy range as in MgO:V^-, it may be assumed that here also $(J_{\alpha\beta_i})/(4U + \epsilon_{i\alpha}) \ll 1$, which justifies the above perturbation approach. From these perturbed wave functions one calculates the transition matrix element to be

$$\langle \alpha' | - e\vec{x} | \beta_i' \rangle \approx (J_{\alpha\beta_i}/4U + \epsilon_{i\alpha})\vec{l} , \tag{3}$$

where $\vec{l}$ is the vector connecting the two O^{2-} ions concerned in the crystal. Contributions from the overlap region of both functions $|\alpha\rangle$ and $|\beta\rangle$ have been neglected because $|\alpha'\rangle$ has a node there. This transition moment can be quite large because of the length of $\vec{l}$, even if $(J_{\alpha\beta_i})/(4U + \epsilon_{i\alpha})$ is small.

In calculating the chemical splitting, only exchange between the final hole states $|\beta_i\rangle$ was taken into account, without considering any change of the ground-state energy. The reason for this being, that the near degeneracy of the final states generally gives a first-order contribution of J_{ij}, whereas the mean energy separation from the ground state, $4U + \epsilon_{i\alpha}$, allows only second-order modifications of the ground level.

In summary, it has been shown that optical

absorption by light-induced transfer of holes clad with their lattice polarization from one to another equivalent lattice site is characterized by three features: (i) The components of the observed bands are Gaussian in shape. Their halfwidths, given by $W^{-1/2} = (8U\hbar\omega_0)^{1/2}$, are related to their peak position, $4U$ (if $\epsilon_{i\alpha} = 0$ and $J_{ij} = 0$). Polaronic bands of holes trapped in the O^{2-} lattice of an oxide material, generally peaked in the visible, thus have typical halfwidths of ~0.5 eV, assuming $\hbar\omega_0 = 0.08$ eV, which corresponds to LO phonon frequencies in such hosts. (ii) The observed line shape results from a superposition of such Gaussian components; their relative positions are given by the eigenvalue differences of the molecular orbitals forming the excited states; their relative intensities depend on the symmetry of these molecular orbitals and on the transition moments to their component wave functions $|\beta_i\rangle|\nu_i\rangle$ as given by the next item. (iii) The intensities of these transitions can be rather strong because of the long dipole arms corresponding to a charge transfer, which counteracts the quenching of exchange by distortion [Eq. (3)].

These features were observed in the optical absorption of MgO:V^-. There the band is peaked at 2.3 eV, its width is ~1 eV; it consists of two exchange-split components separated by 0.1–0.2 eV and its oscillator strength is about 0.1.

2. *Discussison of the spectra*

The absorption bands, P_1 and P_2, correlated with the ESR of center I show the characteristics predicted for the polaronic absorption. Relatively weak ESR signals are accompanied by a rather intense optical absorption, showing the high oscillator strength of the bands. Their positions and widths are comparable to those observed for MgO:V^-.

The dashed curve in Fig. 5 shows a representative band shape for polaron transfer between two oxygen sites. $I(\hbar\omega)\hbar\omega$ [Eq. (2)] has been fitted with $\hbar\omega_0 = 0.1$ eV and $\epsilon_{i\alpha} = 0$ to the maximum of the P_1 band. It appears that the experimental P_1 absorption can be explained by a superposition of such curves. Since the final hole positions in such transfers have different ϵ_i due to their crystallographic inequivalence, such a superposition of slightly shifted bands is expected. There is not enough experimental information on the free parameters in the theory (J_{ij}, $\epsilon_{i\alpha}$, $\hbar\omega_0$, U) to make a theoretical fit by such a superposition meaningful. It can be seen, however, that the characteristic features of the absorption are accounted for by the model.

The P_1 absorption band is thus explained by taking into account only transfers between the p_z orbitals at neighboring O^{2-} sites, nearly equivalent in their orientation towards the defect and therefore nearly equivalent in their energy, see Fig. 9. There is, however, also a finite exchange between the ground-state $O^- p_z$ orbital and the higher-lying O^{2-} orbitals p_x and p_y at neighboring sites. Among the transitions to these orbitals, especially those to p_y are expected to have considerable intensity since these states lie closest to the p_z ground state, ~0.7 eV in the situation where the lattice is stabilized in p_z occupancy, see Sec. III B2. Therefore, the transition moment to the p_y orbitals, analogous to Eq. (3), should not be much smaller than that to the p_z orbitals. We therefore tend to ascribe P_2 to the $p_z - p_y$ transfer described. This interpretation is supported by the fact that the peak energy of P_2 is about 0.5 eV higher than that of P_1, nearly consistent with the above ESR result. In comparing these energies, it should be kept in mind that the energy derived from the ESR applies to the site where the hole is captured, whereas the P_1-P_2 difference belongs to a neighboring site before it has adjusted to the presence of the hole. Because the number of centers II was much smaller than of I, a corresponding absorption could not be definitely identified.

C. Discussion of the additional optical absorption

So far we have given an explanation for the broad optical absorption, P_1 and P_2, of one of the hole traps in $YAlO_3$. From Table II it appears that these holes are created by pumping electrons from the O^{2-} valence states into levels corresponding to bands A, C, D, and F. Not all the holes excited into the valence band in this way, however, are immediately used in the formation of P_1 and P_2. This is shown by the fact that subsequent long-

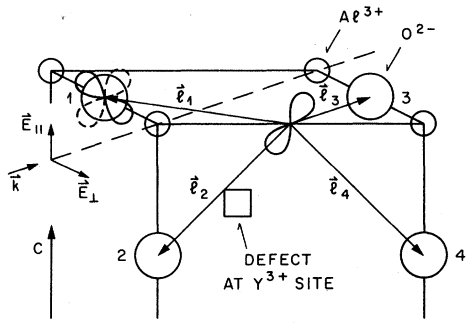

FIG. 9. Relative positions of ions between which the hole can be transferred by light. Again an orthogonal approximation of the $YAlO_3$ lattice is shown. At O^{2-} site 1 the p_z orbital (full) and p_y orbital (dashed) is indicated. The straight arrows $\vec{l}_i$, mark the directions of the transition moments between p_z orbitals at neighboring O^{2-} positions. The used polarization directions of the light are also indicated.

wavelength irradiation increases P_1 and P_2 considerably, apparently by freeing holes intermediately trapped at unknown sites into the valence band from where they can form centers I, responsible for P_1 and P_2.

Nothing is known so far about the chemical nature and physical structure of the additional bands A–F. It is very likely, however, that the absorptions A, D, and F are charge transfer bands since they are quenched by shining into them. Band E seems to be an internal transition of some defect, both because it is rather narrow and because of the rather sharp fine structure on its low-energy wing.

V. CONCLUSION

It has been shown that the light-induced broad-band visible absorption of undoped $YAlO_3$ is correlated to the ESR of holes trapped at O^{2-} ions near defects of the lattice. Depending on the irradiation and thermal history of the crystal two types of centers were observed. As revealed by the analysis of the experimentally determined g and hyperfine tensors, in both cases the holes are trapped in O^{2-} p orbitals pointing towards Y^{3+} sites of the lattice, where presumably unidentified defects are located. In one type of center, the defect seems to be an Y^{3+} vacancy, whereas the charge difference with respect to Y^{3+} is less in the other case. Self-trapping of the hole or rather stabilization by inequivalence of the O^{2-} ions cannot be excluded.

The optical absorption arises because the hole trapping is connected with a lattice distortion. In the light-induced transfer of the hole from one O^{2-} to a structurally equivalent one, the charge carrier is pulled out of its lattice polarization cloud leaving the system in a highly nonstationary excited phonon state. This expresses itself in the appearance of broad absorption bands in the visible. The theory presented includes consideration of the chemical splitting between energetically equivalent final hole states. The most important conclusion reached is that this splitting can be treated without consideration of the phonon system. This appears to be the basis for Watkin's[25] interpretation of the optical absorption of several pseudo-Jahn-Teller systems, where chemical splitting was intuitively founded on group theoretical arguments.

ACKNOWLEDGMENTS

One of the authors (O.F.S.) thanks Dr. A. Räuber for drawing his attention to the study of light-induced coloration of $YAlO_3$. This work would not have been possible without the generous supply of crystals by Dr. H. Opower. We thank Professor K. A. Müller, Professor H. G. Reik, and Professor J. Schneider for discussions and helpful comments on the manuscript. The technical assistance of R. Koch and B. Matthes is gratefully acknowledged.

---

*IBM Postdoctoral Fellow; permanent address: Institut für Angewandte Festkörperphysik der Fraunhofer Gesellschaft, D-78 Freiburg, Federal Republic of Germany.

[1]J. E. Wertz, G. Saville, P. Auzins, and J. W. Orton, J. Phys. Soc. Jpn. 18, Suppl. II, 305 (1963).
[2]Y. Chen and W. A. Sibley, Phys. Rev. 154, 842 (1967).
[3]H. T. Tohver, B. Henderson, Y. Chen, and M. M. Abraham, Phys. Rev. B 5, 3276 (1972).
[4]E. H. Izen, R. M. Mazo, and J. C. Kemp, J. Phys. Chem. Solids 34, 1431 (1973).
[5]L. A. Kappers, F. Dravnieks, and J. E. Wertz, Solid State Commun. 10, 1265 (1972).
[6]M. M. Abraham, Y. Chen, J. L. Kolopus, and H. T. Tohver, Phys. Rev. B 5, 4945 (1972).
[7]B. Henderson and J. E. Wertz, Adv. Phys. 17, 749 (1968); L. E. Halliburton, D. L. Cowan, W. B. J. Blake, and J. E. Wertz, Phys. Rev. B 8, 1610 (1973).
[8]O. F. Schirmer, P. Koidl, and H. G. Reik, Phys. Status Solidi B 62, 385 (1974).
[9]O. F. Schirmer, J. Phys. Chem Solids 32, 499 (1971).
[10]See, e.g., J. Appl. Solid State Phys. 21, 193 (1963).
[11]K. S. Bagdasorov and A. A. Kaminskii, Zh. Eksp. Teor. Fiz. Pis'ma Red. 9, 501 (1969) [JETP Lett. 9, 303 (1969)]; M. J. Weber, M. Bass, K. Andringa, R. R. Monchamp, and E. Comperchio, Appl. Phys. Lett. 15, 342 (1969).
[12]H. Bernhardt, Phys. Status Solidi A 21, 95 (1974).
[13]S. Geller and E. A. Wood, Acta Crystallgr. 9, 563 (1956).
[14]G. Brandt and R. Diehl (unpublished).
[15]K. L. Shaklee and J. E. Rowe, Appl. Opt. 9, 627 (1970).
[16]J. E. Wertz, P. Auzins, J. H. E. Griffiths, and J. W. Orton, Discuss. Faraday Soc. 28, 136 (1959).
[17]M. H. L. Pryce, Proc. Phys. Soc. Lond. A 63, 25 (1950).
[18]O. F. Schirmer, J. Phys. Chem. Solids 29, 1407 (1968).
[19]R. Gazzinelli and R. L. Mieher, Phys. Rev. Lett. 12, 644 (1964); D. Ikenberry, A. N. Jette, and T. P. Das, Phys. Rev. B 1, 2785 (1970); O. F. Schirmer, J. Phys. C 6, 300 (1973).
[20]W. Känzig, J. Phys. Chem. Solids 17, 88 (1960).
[21]See, e.g., F. S. Ham, Phys. Rev. B 8, 2926 (1973).
[22]T. Keil, Phys. Rev. 140, A601 (1965).
[23]M. Lax, J. Chem. Phys. 20, 1752 (1952).
[24]J. H. Van Vleck, *Theory of Electric and Magnetic Susceptibilities* (Oxford U. P., London and New York, 1932).
[25]G. D. Watkins, in *Radiation Effects in Semiconductors*, edited by J. W. Whitehouse (Institute of Physics, London, 1973), p. 228.